Computational Materials Science 50 (2011) 1083–1087

Contents lists available at ScienceDirect

Computational Materials Science

journal homepage: www.elsevier.com/locate/commatsci

Hyperelastic finite element model for single wall carbon nanotubes in tension

E.I. Saavedra Flores [a,*], S. Adhikari [a], M.I. Friswell [a], F. Scarpa [b]

[a] College of Engineering, Swansea University, Singleton Park, Swansea SA2 8PP, United Kingdom
[b] Department of Aerospace Engineering, University of Bristol, Queens Building, University Walk, BS8 1TR Bristol, United Kingdom

ARTICLE INFO

Article history:
Received 1 October 2010
Accepted 4 November 2010
Available online 3 December 2010

Keywords:
Single wall carbon nanotube
Hyperelastic model
Lattice approach
Finite element method

ABSTRACT

This paper investigates the hyperelastic behaviour of single wall carbon nanotubes (SWCNTs) by means of a finite element-based lattice approach. A one-term incompressible Ogden-type hyperelastic model is chosen to describe the mechanical response of SWCNTs under tensile loading. In order to determine the material constants of the model, numerical tests are conducted on a representative arrangement of carbon atoms, establishing equality between the Ogden strain–energy and the variation of the Tersoff–Brenner interatomic potential. The material constants determined here are then used in numerical simulations carried out on SWCNTs models. A good predictive capability of the present model is found when the obtained results are compared to published data. A first conclusion obtained from the present work suggests that a value of 0.147 nm for the C—C bond equivalent diameter is suitable for the hyperelastic description of SWCNTs. A second conclusion reveals a prediction of 0.51 for the breaking strain of SWCNTs under tension, which is in excellent agreement with results obtained from molecular dynamics simulations and continuum theory.

1. Introduction

Since their discovery in the early 1990s [1,2], carbon nanotubes have attracted considerable attention in scientific communities especially due to their extraordinary mechanical properties. Since then, experimental and theoretical techniques have been used in order to investigate the mechanical response of carbon nanotubes. One of these theoretical approaches is the finite element method, a technique which has been used successfully in engineering during the last decades and which has recently been introduced in the analysis of the mechanical deformations of carbon nanotubes [3–6].

In the context of finite element analyses, one of the most popular and simplest ways of modelling carbon nanotubes is the lattice approach [4,7,5,8]. By establishing a linkage between structural and molecular mechanics at the C—C bond level, the lattice approach provides a way to model the deformation of carbon nanotubes by means of conventional finite element analyses using classical beam elements. Curiously, in spite of the extensive work carried out in this context, a review of the current literature on the finite element-based lattice approach shows that most of the research carried out on the constitutive modelling of C—C bonds appears to have been focussed exclusively on the study of reversible behaviour restricted to infinitesimal deformations.

In an attempt to understand the elastic deformation of carbon nanotubes at large strains, our main objective in this paper is to propose an Ogden strain–energy-based hyperelastic constitutive description for the C—C bond mechanical behaviour of SWCNTs subjected to tensile loading. We remark that Ling and Atluri [9,10] have been the first to adopt the Ogden strain–energy density in the context of modelling the SWCNTs mechanical properties. In their approach, the Ogden strain–energy function has been applied in quadratic forms by means of analytical calculations (rather than finite element simulations) on a continuum layer of atoms under uniform deformation state, and with no distinction between tension and compression.

In order to determine a hyperelastic description of C—C bonds, numerical tests are conducted upon a representative arrangement of carbon atoms consisting of one central atom surrounded by three nearest neighbor atoms. By fitting the material constants in the Ogden strain–energy function to the variation of the Tersoff–Brenner interatomic potential, we proceed then to carry out analyses on SWCNTs subjected to tension. By comparing our numerical results to published data, we find that the present model shows a very good predictive capability. In addition, we anticipate that a C—C bond equivalent diameter of 0.147 nm is found to be suitable for the hyperelastic description of SWCNTs. In addition, a breaking strain of 0.51 is predicted by our numerical models, which is in excellent agreement with results obtained by means of molecular dynamics and continuum theory.

The paper is organised as follows. Section 2 describes the hyperelastic modelling of C—C bond mechanical behaviour. The

* Corresponding author. Tel.: + 44 (0)1792 205678; fax: + 44 (0)1792 295157.
E-mail address: e.i.saavedra-flores@swansea.ac.uk (E.I. Saavedra Flores).

0927-0256/$ - see front matter © 2010 Elsevier B.V. All rights reserved.
doi:10.1016/j.commatsci.2010.11.005

validation of the present model is given in Section 3. Section 4 provides the results of analyses carried out on SWCNTs with different geometries. Finally, Section 5 summarises our conclusions.

2. Hyperelastic finite element modelling of the mechanical behaviour of CC bonds

Due to its mathematical simplicity and predictive accuracy for large deformations in conventional materials, an Ogden hyperelastic isotropic material model [11] is chosen for the mechanical response description of C—C bonds. Here, a one-term incompressible version of the Ogden strain–energy density function is adopted, whose expression is given by

$$\Psi = \frac{2\chi}{\alpha^2}\left\{(\lambda_1)^\alpha + (\lambda_2)^\alpha + \frac{1}{(\lambda_1\lambda_2)^\alpha} - 3\right\}, \tag{1}$$

where λ_1 and λ_2 are the first and second principal stretches and χ and α are material constants. Here, perfect incompressibility has been assumed, so that the third principal stretch λ_3 has been expressed as a function of λ_1 and λ_2 by means of the volumetric constraint $\lambda_1\lambda_2\lambda_3 = 1$. In addition, if the uniaxial deformation state is taken into consideration, the second and third principal stretches can be calculated in terms of λ_1 as

$$\lambda_2 = \lambda_3 = \frac{1}{\sqrt{\lambda_1}}, \tag{2}$$

and consequently, the strain–energy density function (1) can be rewritten as

$$\Psi = \frac{2\chi}{\alpha^2}\left\{(\lambda_1)^\alpha + \frac{2}{(\lambda_1)^{\frac{\alpha}{2}}} - 3\right\}. \tag{3}$$

In order to describe the mechanical response of C—C bonds, we proceed to fit the constants χ and α in Eq. (3) according to the variation of the Tersoff–Brenner interatomic potential [12,13]. The corresponding expression for this interatomic energy is defined by

$$V_B(r_{ij}) = V_R(r_{ij}) - B_{ij}V_A(r_{ij}), \tag{4}$$

where r_{ij} is the distance between atoms i and j, and V_R and V_A the repulsive and attractive pairs of energy terms. The parameter B_{ij} represents a multi-body coupling between atoms i and j and the local environment surrounding these atoms. The commercially available Material Studio Software [14] and its tool Gulp [15] are used to perform the calculation of the Tersoff–Brenner potential. In all cases, the equilibrium bond length between carbon atoms is assumed to be 0.142 nm [6].

In the present paper, we choose two possible deformation modes to be analysed in a representative arrangement of carbon atoms (as shown in Fig. 1). The present arrangement consists of one central carbon atom surrounded by three neighbor atoms. If we adopt an equivalent mechanical system, the first (Fig. 1a) and second deformation modes (Fig. 1b) correspond to compression and tension in one of the (bonding) structural elements, respectively, keeping fixed the remaining degrees of freedom. The C—C bond equivalent diameter adopted here is 0.147 nm.

The determination of the Ogden model constants for each of the deformation modes is presented in the following.

(i) *First deformation mode*
The corresponding variation of Tersoff–Brenner interatomic potential (with respect to the initial value, when the system is undeformed) and the fitted Ogden strain–energy function are shown in Fig. 2. The horizontal axis indicates the axial stretch (λ_1), defined as the ratio between the current length of the corresponding bonding element and its original length. The vertical axis provides the amount of stored energy during the compression (and also tensile) deformation process and the variation of the interatomic bonding energy. In order to fit the Ogden strain–energy function to the variation of the interatomic potential, we use Eq. (3) multiplied by the volume (in the *reference* configuration) of the bonding element under deformation. The resulting material constants obtained for this first deformation mode are

$$\chi = 1166.18 \text{ GPa and } \alpha = -10.0. \tag{5}$$

Importantly, the mean squared error registered here is 0.0299, for a range of axial stretch between 0.675 and 1.0.

(ii) *Second deformation mode*
The fitted Ogden strain–energy to the variation of the Tersoff–Brenner potential in this second deformation mode is also shown in Fig. 2. Here, the resulting material constants obtained for the Ogden strain–energy are

$$\chi = 2332.36 \text{ GPa and } \alpha = -14.0. \tag{6}$$

Here, the mean squared error is 0.0177 for an axial stretch ranging between 1.0 and 1.33. Note also that we have truncated the axial tensile stretch in the Ogden strain–energy (second deformation mode) to 1.33 due to the effective range

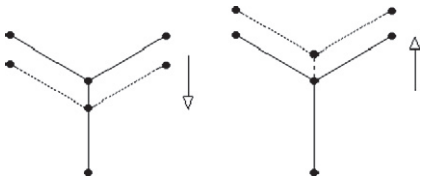

(a) First deformation mode: Shortening of the distance between two neighbor atoms.

(b) Second deformation mode: Separation of two neighbor atoms

Fig. 1. Two possible deformation modes in a representative arrangement of carbon atoms.

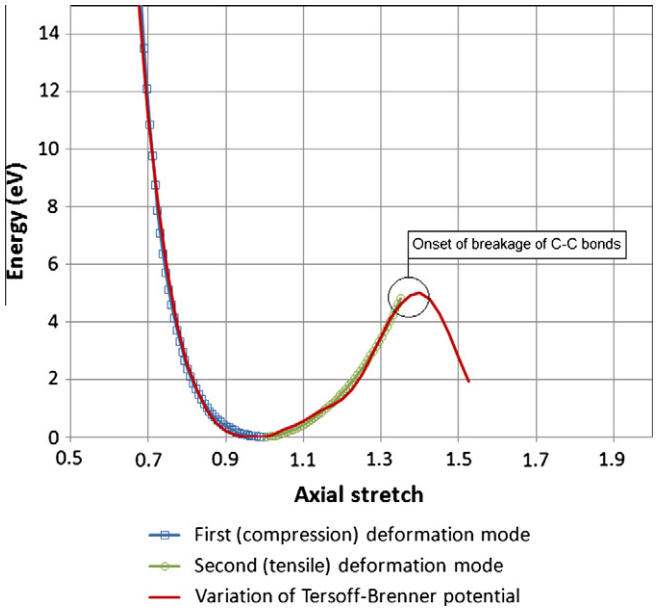

Fig. 2. Ogden strain–energy fitted to the variation of the Tersoff–Brenner interatomic potential. Note that axial stretch (in second deformation mode) has been truncated to 1.33 which is interpreted as the onset of breakage of C—C bonds.

of the cut-off function in the Tersoff–Brenner potential, which is interpreted physically as the onset of breakage of C—C bonds.

We remark here that isotropic conditions have been assumed in the constitutive modelling of C—C bonds when adopting the Ogden hyperelastic description. Therefore, the strain–energy of the equivalent mechanical system undergoing other possible deformation modes, such as angular deformation, bending and torsion, is calculated under the standard isotropic constitutive formulation. The approximation provided by the above type of isotropic model represents a first approximation to the phenomenological modelling of the complex (and sometimes intricate) interatomic interactions at large strains.

3. Validation of the model

Our purpose in this section is to validate the material constants obtained in the previous section with published data. Here, we choose the information compiled by Ling and Atluri [9,10], consisting of an axially stretched armchair SWCNT.

We use the commercial finite element software Abaqus [16] in order to carry out our simulations. We perform an analysis of a (10,10) SWCNT model with 4.92 nm initial length. The finite element mesh consists of 820 nodes and 1210 beam elements. We select the two-noded hybrid beam element, type B31H, in Abaqus. Transverse shear strains (Timoshenko beam theory) are considered in the beam element formulation. Here, the Z axis corresponds to the axial (longitudinal) direction of the tube, whereas X and Y correspond to the transversal directions. Boundary conditions are imposed on the nodes located at $Z = 0$, allowing radial displacements only. Prescribed displacements in the longitudinal direction are applied on nodes located at $Z = 4.92$ nm equal to 0.15 of the initial length of the tube. Fig. 3 shows the deformed shape of the SWCNT at the end of the loading programme (0.15 axial strain). Prescribed displacements and boundary conditions are also indicated.

The Ogden strain–energy per atom is calculated for the SWCNT and shown in Fig. 4. The corresponding curves show a good agreement between our numerical prediction and the results reported in [17] (based on molecular dynamics simulations), [9,10] (atom-based cell model), [18] (structural mechanics approach), [19] (Molecular dynamics), [20] (Molecular mechanics) and [21] (Molecular dynamics), which demonstrates the good predictive capabilities of the present model.

We remark that although Ling and Atluri [9,10] provided a hyperleastic description of SWCNTs, the results reported by them and shown in Fig. 4 do not include this hyperelastic formulation. Instead, they used another approach to calculate this curve by minimising the Helmholtz free energy via the local harmonic approach [22] and using the Tersoff–Brenner potential directly in an atom-based cell model.

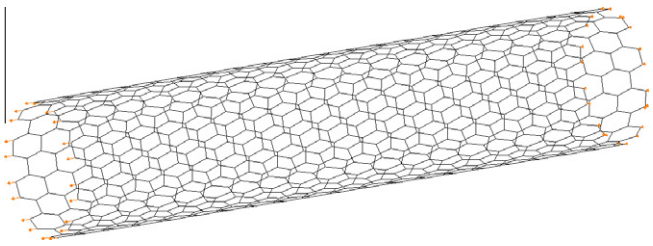

Fig. 3. Deformed finite element mesh of a (10,10) SWCNT with 4.92 nm (initial) length, under tensile loading.

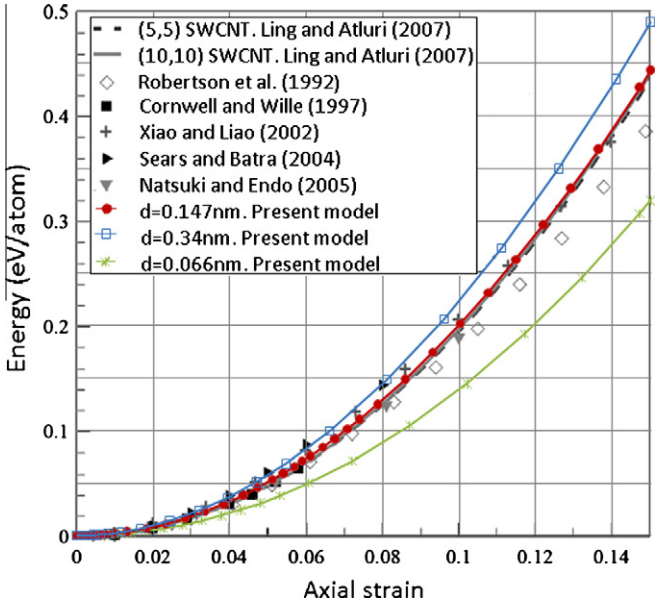

Fig. 4. Ogden strain–energy per atom for an armchair (10,10) SWCNT with 4.92 (initial) length, and variation of Tersoff–Brenner potential from other authors.

4. Numerical results for single wall carbon nanotubes

In order to investigate the consequences of choosing other equivalent diameters in the procedure described in the present work, we consider two different diameters in the example from Section 3. The first value is 0.34 nm and was reported by Li and Chou [4]. Assuming this value, the material properties found suitable for fitting the Ogden strain–energy function are $\chi = 217.99$ GPa and $\alpha = -10.0$, for the first deformation mode, and $\chi = 435.989$ GPa and $\alpha = -14.0$, for the second mode. The second diameter is 0.066 nm and was reported by Yakobson et al. [23]. Considering this value, the suitable constants for fitting the Ogden strain–energy function are $\chi = 5785.124$ GPa and $\alpha = -10.0$, for the first mode, and $\chi = 11{,}570.25$ GPa and $\alpha = -14.0$, for the second deformation mode. For these two additional sets of parameters, we calculate the Ogden strain–energy curves, as shown in Fig. 4. From these results, we can observe the lack of agreement between the strain–energy curves and the variation of

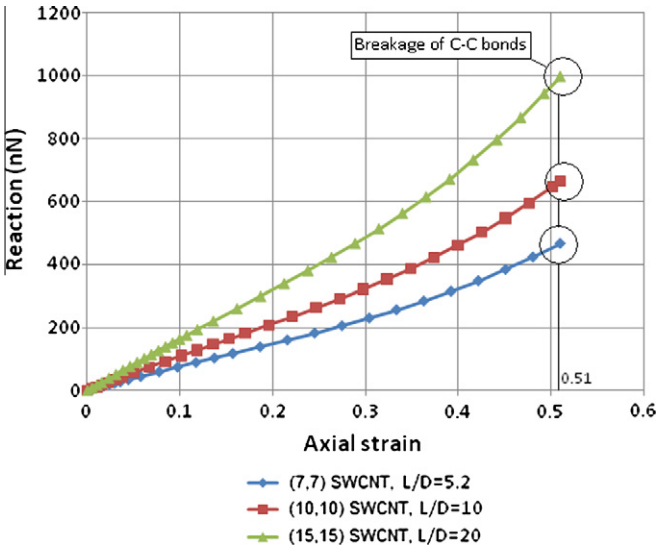

Fig. 5. Variation of the total reaction at the fixed end of three different SWCNTs. Breaking strain of 0.51 is also indicated.

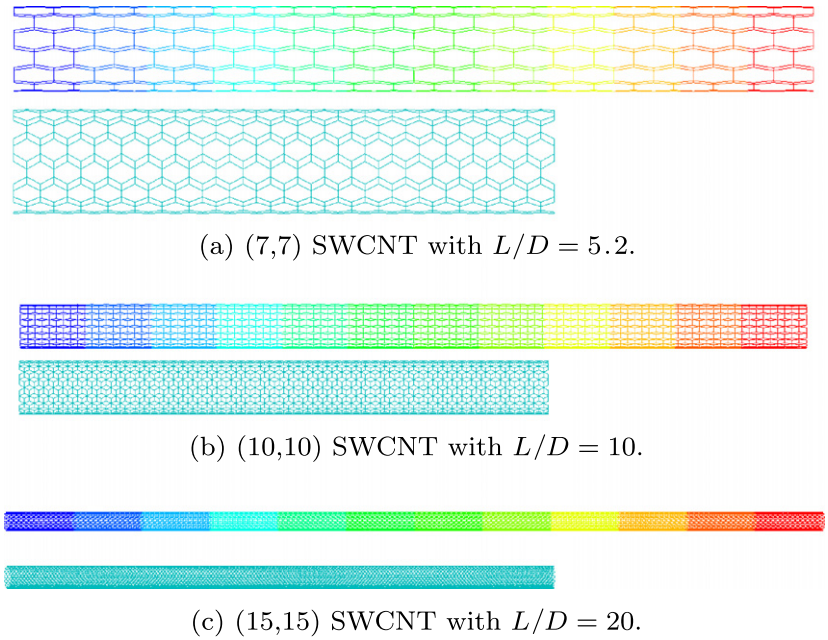

Fig. 6. Three SWCNTs under tensile loading with their deformed and undeformed shapes (not to scale).

the Tersoff–Brenner potential when other diameters different to 0.147 nm are adopted in the analyses. We note that Tserpes and Papanikos [5] also obtained the same value of diameter (0.147 nm) in their calculations in the context of infinitesimal strains. However, they did not take into consideration the shear effects present in the deformation of (thick) beams.

Further, we explore the variation of the total reaction at the fixed end of the carbon nanotube for three new geometries. The equivalent diameter chosen here is again 0.147 nm. The first geometry corresponds to a (7,7) SWCNT with a ratio between initial length, L, and initial diameter, D, equal to $L/D = 5.2$. The finite element mesh consists of 574 nodes and 847 elements. The prescribed displacement applied here is 2.5 nm in the axial direction. The next geometry is a (10,10) SWCNT with $L/D = 10$. The finite element mesh consists of 2220 nodes and 3310 elements and the prescribed displacement is 6.9 nm. Finally, the last case is a (15,15) SWCNT with ratio $L/D = 20$ and a mesh with 9930 nodes and 14,865 beam elements. The prescribed displacement here is 20.71 nm. For these three cases, the same boundary conditions adopted in Section 3 are used.

Fig. 5 shows the variation of the total reaction obtained for the three new geometries analysed here. In addition, Fig. 6a–c shows the corresponding undeformed and deformed (at the end of the loading programme) finite element meshes and also the contour diagrams for the displacement field in the axial (longitudinal) direction. The colours range varies from blue[1], with zero displacements, to red, when the maximum applied displacement is reached in each simulation.

From the graph shown in Fig. 5, it is possible to observe a stiffer overall mechanical response for higher L/D ratios. In addition, the three SWCNTs show an almost linear range up to 0.05 axial strain, with little variation in the slope of their corresponding curves. For larger strains, a stiffening effect can be observed in the three curves, attributed to the geometric alignment of the C—C bonding elements along the longitudinal direction (direction in which the prescribed displacements have been applied). This effect is possible to observe since large strains/displacements have been taken into account in our computational simulations. A second reason for this effect is the use of the Tersoff–Brenner formulation as interatomic potential, which provides a stiffer mechanical response when compared to other standard potentials. Sears and Batra [20] noticed this when comparing Tersoff–Brenner potential with Morse formulation for strains over 20% under bond stretching.

By inspecting the numerical results (not shown here), we also note that in the three cases analysed here, an increase of 1.33 in the (C—C bond) length is reached between at least two neighbor nodes when an axial strain of 0.51 is applied in the carbon nanotubes (we remind the reader that in Section 2 we limited the axial tensile stretch to 1.33 due to the onset of breakage of C—C bonds). This important observation suggests that for axial strains over 0.51, some of the C—C bonds in the SWCNTs will start to break and to lead to a partially irreversible nonuniform deformation. Importantly, the breaking strain of 0.51 predicted here agrees very well with the breaking strain of 0.55 reported by Yakobson et al. [24], using molecular dynamics at a low temperature (50 K), and with the value of 0.52 calculated by Zhang et al. [25], using continuum theory. As noticed by Zhang et al. [25], we remark that a low temperature has been chosen to compare our results with those obtained by Yakobson et al. [24] since the Tersoff–Brenner potential in Section 2 does not take into account temperature effects.

In order to assess the order of magnitude of the reactions given in Fig. 5, we compare these results with experimental data. Unfortunately, little information about tensile strength has been reported at this level of deformation and low temperature. Nevertheless, Yu et al. [26] provided a range of values between 13 and 52 GPa, in ropes of SWCNTs, for strain values of 5.3% or lower. In this experimental work, the authors assumed that all SWCNTs in the ropes studied were (10,10) nanotubes (1.356 nm diameter) with 0.34 nm wall thickness. Since the thickness (C—C bond diameter) adopted in the present work is 0.147 nm, we proceed to multiply the range of stresses 13–52 GPa by a factor of 2.31, obtained as the quotient between 0.34 nm and 0.147 nm. This provides a new consistent range which results between 30 and 120 GPa. In our simulations, the reaction obtained in the (10,10) SWCNT for a 5% strain is 54.9 nN, which results in a stress of 87.7 GPa when an area $A = 1.356 \cdot \pi \cdot 0.147 = 0.6262\ \text{nm}^2$ is

[1] For interpretation of colour in Fig. 6, the reader is referred to the web version of this article.

considered, demonstrating a good agreement between our numerical predictions and experimental data. Despite the values reported by Yu et al. were determined for a different temperature, this comparison is possible since the magnitude of the tensile stresses do not depend significantly on temperature changes [10].

5. Conclusions

The hyperelastic behaviour of single wall carbon nanotubes (SWCNTs) has been investigated by means of a finite element-based lattice approach. A one-term incompressible Ogden-type hyperelastic model has been chosen for the mechanical response prediction of SWCNTs under tensile loading. Numerical tests have been conducted on representative arrangements of carbon atoms in order to determine material constants of the model. Finite element simulations have been carried out on SWCNT models introducing such material properties. The results have been compared to published data, demonstrating the predictive capability of the present model. A first important conclusion in the present work suggests that a value of 0.147 nm for the C—C bond equivalent diameter is suitable for the hyperelastic modelling of SWCNTs. A second conclusion reveals a prediction of 0.51 for the breaking strain of SWCNTs under tension, which is in excellent agreement with those results obtained from molecular dynamics and continuum theory.

Acknowledgement

The authors acknowledge funding from the European Research Council through Grant No. 247045 entitled "Optimisation of Multiscale Structures with Applications to Morphing Aircraft".

References

[1] S. Ijima, Nature 354 (1991) 56–58.
[2] S. Ijima, T. Ichihashi, Nature 363 (1993) 603–605.
[3] M. Arroyo, T. Belytschko, International Journal for Numerical Methods in Engineering 59 (2004) 419–456.
[4] C. Li, T. Chou, International Journal of Solids and Structures 40 (2003) 2487–2499.
[5] K.I. Tserpes, P. Papanikos, Composites Part B: Engineering 36 (2005) 468–477.
[6] F. Scarpa, S. Adhikari, Journal of Physics D: Applied Physics 41 (2008) 085306.
[7] F. Scarpa, S. Adhikari, C. Remillat, Nanotechnology 21 (2010) 125702.
[8] A. Kalamkarov, A. Georgiades, S. Rokkam, V. Veedu, M. Ghasemi-Nejhad, International Journal of Solids and Structures 43 (2006) 6832–6854.
[9] X. Ling, S. Atluri, Journal of Applied Physics 101 (2007) 064316.
[10] X. Ling, S. Atluri, Computer Modelling in Engineering and Science 21 (2007) 81–91.
[11] R.W. Ogden, Non-linear Elastic Deformations, Ellis Horwood, Chichester, 1984.
[12] D. Brenner, Physical Review B 42 (1999) 9458–9471.
[13] J. Tersoff, Physical Review B 37 (1988) 6991–7000.
[14] Material Studio, Release Notes, Release 4.3, Accelrys Software Inc., San Diego, USA, 2008.
[15] J. Gale, A. Rohl, Molecular Simulation 29 (5) (2003) 291–341.
[16] Abaqus, Theory Manual, Version 6.4, Hibbitt, Karlsson and Sorensen, Inc., Rhode-Island, USA, 2002.
[17] C. Corwell, L. Wille, Solid State Communications 101 (1997) 555–558.
[18] T. Natsuki, M. Endo, Applied Physics A 80 (2005) 1463–1468.
[19] D. Robertson, D. Brenner, J. Mintmire, Physical Review B 45 (1992) 12592–12595.
[20] A. Sears, R. Batra, Physical Review B 69 (2004) 235406.
[21] T. Xiao, K. Liao, Physical Review B 66 (2002) 153407.
[22] R. LeSar, R. Najafabadi, D. Srolovitz, Physical Review Letters 63 (1989) 624–627.
[23] B. Yakobson, C. Brabec, J. Bernholc, Physical Review Letters 76 (1996) 2511–2514.
[24] B. Yakobson, C. Brabec, J. Bernholc, Computational Materials Science 8 (1997) 341–348.
[25] P. Zhang, Y. Huang, H. Gao, K. Hwang, Journal of Applied Mechanics 69 (2002) 454–458.
[26] M. Yu, B. Files, S. Arepalli, R. Ruoff, Physical Review Letters 84 (24) (2000) 5552–5555.